IJES *Iranian Journal of Earth Sciences*
Vol. 11, No. 1, 2019, 80-92.

Delineation of hydrothermal alteration zones for porphyry systems utilizing ASTER data in Jebal-Barez area, SE Iran

Sara Fakhari*[1], Alireza Jafarirad[1], Peyman Afzal[2], Mohammad Lotfi[3]

1. Department of Geology, Science and Research Branch, Islamic Azad University, Tehran, Iran
2. Department of Petroleum and Mining Engineering, South Tehran Branch, Islamic Azad University, Tehran, Iran
3. Department of Geology, North Tehran Branch, Islamic Azad University, Tehran, Iran

Received 29 April 2017; accepted 3 October2018

Abstract
The Urumieh-Dokhtar Magmatic Belt (UDMB) is the host of many Iranian Cu porphyry deposits. The southern part of this belt, in the Jebal-Barez area, has been less investigated due to the mountainous and rough topography as well as some security confrontations. Porphyry deposits are associated with hydrothermal alteration zones, which can be mapped using the remote sensing data such as Advanced Space borne Thermal Emission and Reflection Radiometer (ASTER). The aim of this study was to identify and detect the alteration zones associated with porphyry systems using ASTER data in Jebal-Barez area, SE Iran. For this reason, seven scenes of ASTER level-1B data which cover the Jebal-Barez area, were pre-processed and then processed by band ratio, false color composite and Spectral Angle Mapper (SAM) methods. The result indicated the presence of extensive phyllic and argillic alteration zones. The argillic alteration is surrounded by border zones of propylitic alteration. Also, a massive granitoid intrusion in NW of the studied area was detected by SAM method and the color composite of 4, 6, and 8 bands of ASTER as a completely altered area (SF area) which strongly needs more detailed exploration and field inspections.
Keywords: *ASTER, Band ratio, False colour composite, Spectral Angel Mapper (SAM), Alteration, Jebal-Barez.*

1. Introduction
Porphyry copper deposits contain most of the world's Cu, Mo resources and about 20% of the world's Au and minor amounts of other metals, especially, Ag, Pd, Te, Se, Bi, Zn and Pb (Sillitoe and Gape 1984; Sillitoe 2010; Alimohammadi et al. 2015).Furthermore, all the known porphyry deposits in Iran occur within Urumieh-Dokhtar Cenozoic magmatic belt (Shafiei et al. 2009; Asadi et al. 2014). Actually, the SE part of this magmatic belt is named Kerman Cenozoic magmatic arc (Shafiei et al. 2009). Jebal-Barez region is situated in this arc which is shallow crustal depth and related to an extensive hydrothermal alteration (Lowell and Guilbert 1970; Mars 2010; Alimohammadi et al. 2015). Hydrothermal alteration zones are the main evidences for prospectively mapping of porphyry deposits. Lowell and Guilbert (1970) described the mineral zones and hydrothermal alterations of porphyry copper deposits with a core of quartz, and potassium-bearing minerals surrounded by multiple zones containing phyllic, potassic, argillic, and propylitic alterations, respectively (Fig 1). In this model, the propylitic zone, which surrounds the other zones, has been developed from the surface to deeper levels. The sericitic, and especially the advanced argillic alterations are much less in expansion and related to the alkaline and calc-alkaline intrusions, respectively (e.g., Meyer and Hemley 1967; Lang et al. 1995; Sillitoe 2002; Holliday and Cooke 2007).

*Corresponding author.
E-mail address (es): sara.fakhari@yahoo.com

Commonly, the sericitic alterations of the porphyry copper deposits totally coat or partially overwhelm the potassic and chlorite-sericite cumulations, although the sericitic halos are zoned to the chlorite-sericite alterations evidently. The Advanced Space borne Thermal Emission and Reflection Radiometer (ASTER) is an advanced multispectral satellite imaging system that has been created for mapping the geological structures and delineating definite alteration minerals (Rowan et al. 2003; Mars and Rowan 2006; Alimohammadi 2015). This system includes three different subsystems with a total of 14 bands. Therefore, the visible near infrared (VNIR) subsystem captures the optical images of three bands (0.52 – 0.86 μm), with spatial resolution of 15 m, while the shortwave infrared (SWIR) subsystem obtains optical images of six bands (1.60 – 2.43 μm), with spatial resolution of 30 m, and finally the thermal infrared (TIR) subsystem captures the optical images of five bands (8.12 – 11.65 μm), with a spatial resolution of 90 m. Moreover, this system has a backward-looking VNIR telescope with a resolution of 15 m (Table 1; Rowan and Mars 2003). The aim of this study was to identify the alteration zones related to the copper porphyry deposits by detecting the altered minerals from ASTER data. In addition, seven scenes of ASTER cover this area. These were obtained on 09/06/2001, 24/05/2001, and 15/05/2001. Processing methods are band ratio, false color composite and Spectral Angle Mapper (SAM) methods.

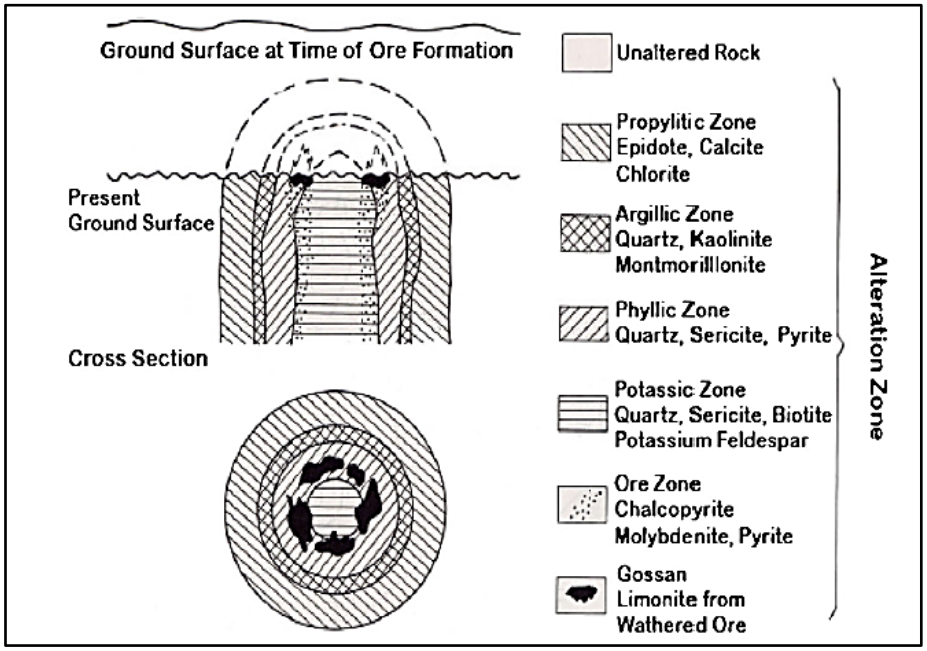

Fig 1 Schematic model of hydrothermal alteration zones related to porphyry copper deposits containing propylitic, argillic, phyllic, and potassic alterations (Lowell and Guilbert 1970; Hedenquist et al. 2000)

Table 1. Sensor characteristics of ASTER instruments (summarized from Sabins 1999; Rowan and Mars 2003)

Spectrum	Band	Spectral domain (µm)	Radiometric resolution (bits)	Spatial resolution (m)
VNIR	1	0.520-0.600	8	15
	2	0.630-0.690	8	15
	3N	0.780-0.860	8	15
	3B	0.780-0.860	8	15
SWIR	4	1.600-1.700	8	30
	5	2.145-2.185	8	30
	6	2.185-2.225	8	30
	7	2.235-2.285	8	30
	8	2.295-2.365	8	30
	9	2.360-2.430	8	30
TIR	10	8.125-8.475	12	90
	11	8.475-8.825	12	90
	12	8.925-9.275	12	90
	13	10.25-10.95	12	90
	14	10.95-11.65	12	90

2. Materials and methods

2.1. Geological setting of study area

One of the major important potential for porphyry deposits in the world is the Urumieh Dokhtar Cenozoic magmatic belt (UDCMB). Moreover, this magmatic belt is a host for porphyry and vein-type Cenozoic Copper (± Mo & Au) mineralization. In addition, the KCMA contains copper deposited especially in Jebal-Barez in the SE part of KCMA (Fig 2). Copper deposits in the KCMA are closely related to Miocene porphyry. Copper deposits were intruded and emplaced into Eocene volcanic-sedimentary successions (Hezarkhani 2006; Shafiei 2010; Afzal et al. 2016; Daneshvar Saein and Afzal, 2017). The oldest rocks in Jebal-Barez are Certaceous and Eocene flysch deposits, and on the other hand, the youngest rocks are Quaternary alluvial deposits and gravel fans. The lower Eocene rocks are parts of volcanic complex including rhyolitic lavas, breccias, acidic tuffs and pyroclastic rocks (Fig 2; Shafiei et al. 2009; Honarmand et al. 2011).

In this district, many kinds of porphyry and vein-type copper occurrences /deposits exist. Therefore, porphyry type mineralization is located in the upper parts of the intrusive rocks and also vein-type mineralization is controlled by different trends faults and is found in both intrusions and fine grained volcanic rocks (Honarmand et al. 2011; Asadi et al. 2014; Afzal et al. 2016).

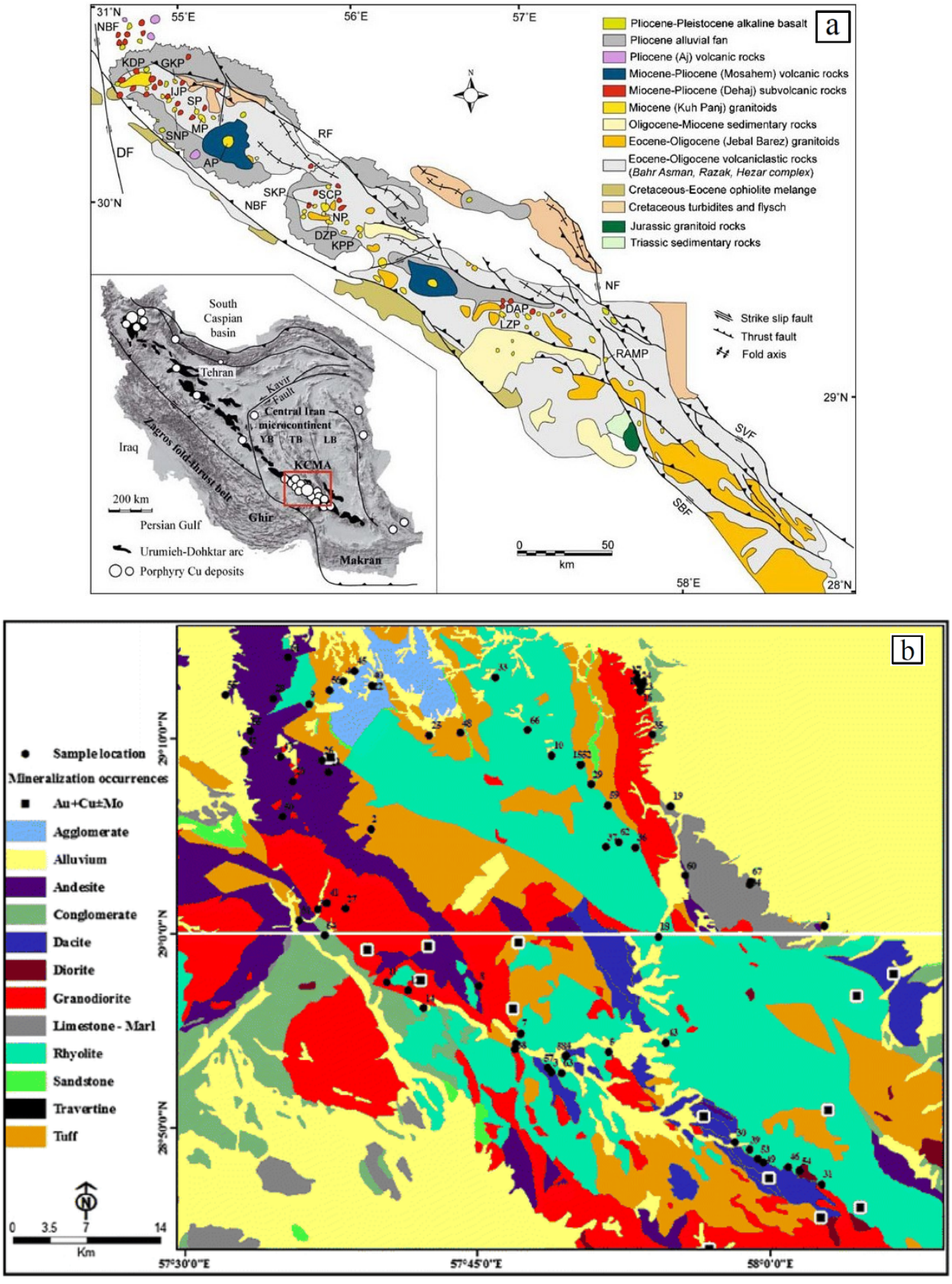

Fig 2. a) Geological map for Kerman Cenozoic Magmatic Belt (KCMB) and its situation in the UDMB (Shafiei et al. 2009); b) Geological map of Jebal-Barez area (Pazand and Javanshie, 2015).

2.2. Mineralization and Alteration

In the Jebal-Barez area, malachite, azurite, chalcopyrite and chalcocite with barite and galena can be observed as metallic mineralization. Mineralization occurs as quartz stock works, vein and disseminated sulphides (Fig 3) in both the Oligocene-Miocene porphyritic stocks and Eocene mafic and also intermediate volcanic rocks. In addition, common hypogene mineral ores in this area are chalcopyrite and pyrite with molybdenite, bornite and magnetite (Dimitrijevic 1973; Shafiei 2010; Honarmand et al. 2011). Four distinct types of alterations are recognized at this area: potassic, phyllic, argillic and propylitic. Fig. 3a shows the argillic alteration and Fig. 3b illustrates Epidotic veins in Propylitic alteration zone of dacitic tuff. Argillic alteration plays a key role in the formation of clay minerals, including kaolinite, smectite and illite. This is generally a low temperature event, and some may occur in atmospheric conditions. Outcrops of copper mineralization in the Jebal-Barez are mostly vein type and their thickness varies. One of these veins, with 50m length, is the andesite unit (Ea) and part of it can be found in Fig. 3c. The surface of this vein is dark due to iron oxide. Another Sample of these outcrops which is siltstone and sandstone unit (Es) is shown in Fig. 3d. Characteristics of the major copper prospects in the study area are presented in Table 2. Rock types of the study area include intensely hydrothermal alteration zones (Table 2). Main copper mineralization are accumulated with potassic, quartz sericitic (phyllic), silicic, propylitic and locally argillic alteration (Fig 3a). All samples which have been collected during the field observations were analysed with XRD methods and ICP for correlating remote sensing results.

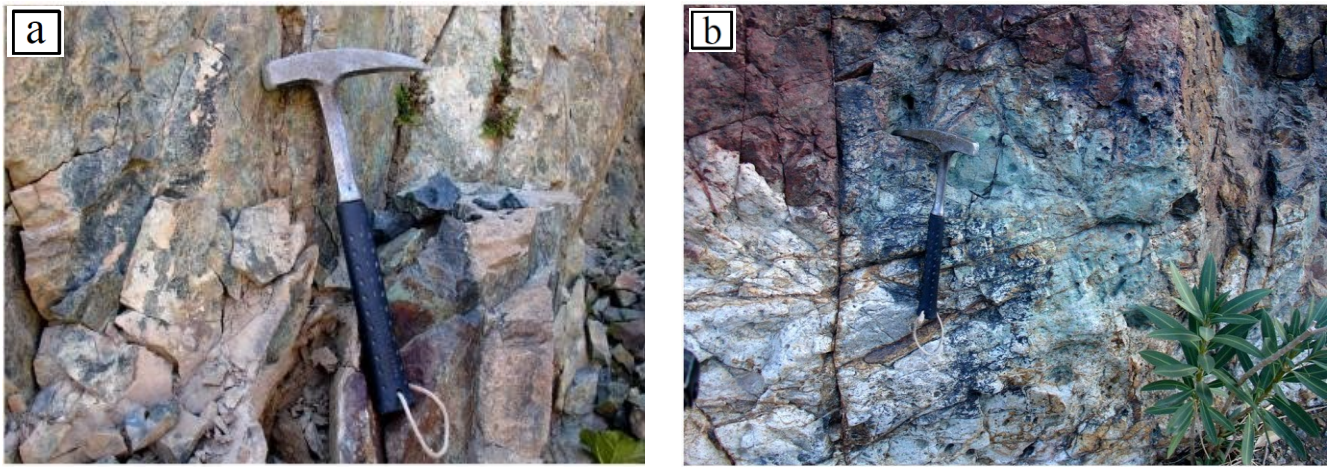

Fig 3. Copper mineralization in the studied area, a) mineralization in a sulfidic vein b) copper dissimination in argillic alteration zone: E^{da}

2.3. ASTER image pre-processing

Seven scenes of ASTER cover the study district and in these scenes, pre-processing is necessary. In this study, nine bands of ASTER were used so each band has specific features (Table 1) and the ASTER has more bands compare with ETM^{+}. Moreover, there are six bands of shortwave infrared of this imaging system and processing of this image can delineate and identify minerals of copper in each zone in the Jebal-Barez area. This method can be used for geological field works which does not have too much vegetation and this region has low vegetation. In the seven scenes pre-processing, is necessary to observe spatially and radiometrically corrected images in order to analyse and compare spectral data. Each raw image must be converted to an ortho-image for geometric correction. Geometric and radiometric correction has been applied by generating a Digital Elevation model (DEM) based on topographic data and using ground control points in the orthorectification of ASTER images and also, radiometric correction is used for making certain high-quality information from remote sensors. The images were pre-georeferenced to UTM zone 40 north projections using the WGS-84 datum. The shortwave infrared data could be affected by the 'crosstalk' instrument problem. In this case, this problem is an additive error in radiance due to the leakage of photons from one detector element to another (Rowan and Mars

Table 2.Characteristics of the major copper prospects in the study area

Prospect name	Mineralization type	Main alteration types	Main alteration minerals	Main ore minerals
Desk	Vein	Phyllic, ilicification, Argillic, arositization	Muscovite, Quartz, Kaolinite, Jarosite	Pyrite
Dashteravan	Vein	Quartz sericite, Silicification,Propylitic, Argillic,Jarositization, Pyritization	Muscovite, Quartz, Chlorite, Epidote, Kaolinite, Jarosite	Pyrite, Malachite, Magnetite
Mijan	Porphyry and Vein	Argillic, Quartz sericite,Potassic, Silicification, Pyritization, Jarositization, Propylitic	Quartz, Kaolinite, Muscovite Montmorillonite, Illite, Chlorite, Calcite	Pyrite, Malachite, Azurite, Chalcopyrite, Magnetite, Hematite
Gerduchaharshanbeh	Porphyry and Vein	Quartz sericite, Argillic, Propylitic, Potassic	Muscovite, Illite, Quartz, Kaolinite, Chlorite, Montmorillonite, Epidote	Pyrite, Malachite, Chalcopyrite, Azurite, Magnetite
Hishin	Vein	Quartz sericite, Argillic, Jarositization, Silicification, Potassic	Muscovite, Quartz, Albite,Orthoclase, Kaolinite,Calcite,	Pyrite, Malachite, Hematite,Azurite, Chalcopyrite
Kerver	Porphyry	Potassic, Quartz sericite, Propylitic, Hematitization, Silicification, Biotitization, Pyritization	Muscovite, Quartz, Jarosite,Albite, Orthoclase, Kaolinite, Epidote, Chlorite, Calcite,Biotite	Pyrite, Malachite, Chalcopyrite, Bornite, Azurite, Magnetite, Goethite
Lordkhizan	Porphyry and Vein	Phyllic, Silicification, Potassic, Propylitic	Muscovite, Illite, Quartz,Biotite, Albite, Orthoclase,Kaolinite, Chlorite, Calcite	Pyrite, Chalcopyrite, Malachite, Tetrahedrite, Hematite,Chalcocite
Banehrizan	Vein	Phyllic,Silicification, Argillic, Propylitic, Hematitization, Pyritization, Biotitization, Tourmalinization	Muscovite, Illite, Quartz, Albite, Kaolinite, Epidote, Amphibole, Chlorite, Biotite,Tourmaline	Pyrite, Chalcopyrite, Malachite, Bornite, Magnetite, Molybdenite, Hematite
Sartuk	Vein	Argillic, Silicification,Phyllic, Pyritization,Hematitization	Kaolinite, Quartz, Muscovite	Pyrite, Hematite, Goethite
Reagan	Porphyry and Vein	Quartz sericite, Propylitic, Silicification, Hematitization, Jarositization	Muscovite, Illite, Quartz, Albite, Chlorite, Epidote, Calcite	Pyrite, Malachite, Azurite, Chalcopyrite, Magnetite, Goethite

2003; Alimohammadi et al. 2015). The atmosphere correction has been used because of dust and other things which exist in the atmosphere and that are the reason for errors during imaging from earth surface.

2.4. Data processing

The sensitivity step of remote sensing is image processing which has effect on final results. The aim of remote sensing in this study is delineation of clay minerals, propylitic, silicic and iron oxides for detecting alteration zones. Therefore, image processing was used to find and detect alterations in the Jebal-Barez area. In this study, various remote sensing analysis techniques have been applied consisting of Band ratio (Sabins, 1999), false color composite, Spectral Angle Mapper (SAM–Honarmand et al. 2011; Zoheir and Emam 2012; Aramesh Asl et al. 2015) by the PCI Geomatica version 9.1 and ENVI (Environment for Visualizing Images) version 4.8 softwares.

2.4.1. Band ratio

Band ratio is used to reduse sun light, topography effects and also for illustrating information of images spectral. This method is designed to display the spectral contrast of specific absorption features which has been widely utilized in geological remote sensing (Rowan et al. 2006). Image spectral reflectance of clay mineral showed in band nine has the highest reflection and in bands four and seven, it has high reflection; otherwise, in band five, it has moderate reflection (Fig 4). 3/2 band ratio can be musk vegetation in this area (Fig 5). Among the diverse band ratios such as 4/9, 5/9, and 7/9 which is detected alteration area, we can apply the band ratio of Table 3 as the best choice for identifying hydrothermal alteration zones (Figs 6 to 8).

Table 3. ASTER band ratio to detect Alteration

Feature	Band Ratio	Reference
Argillic alteration	4+6)/5(	Rowan(USGS)
Phyllic alteration	5+7)/6(	
Carbonate/chlorite/epidote	7+9)/8(	Rowan

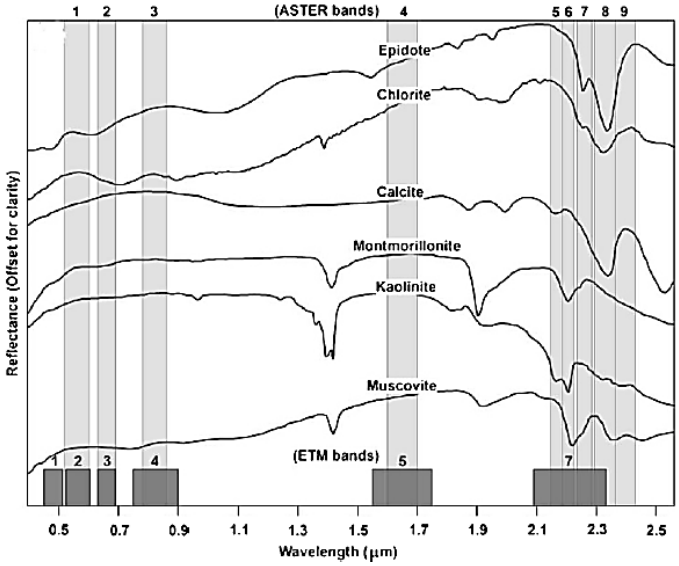

Fig 4. Spectral library of reflectance of important hydrothermal alteration minerals (Rowan et al. 2006; Honarmand et al. 2011).

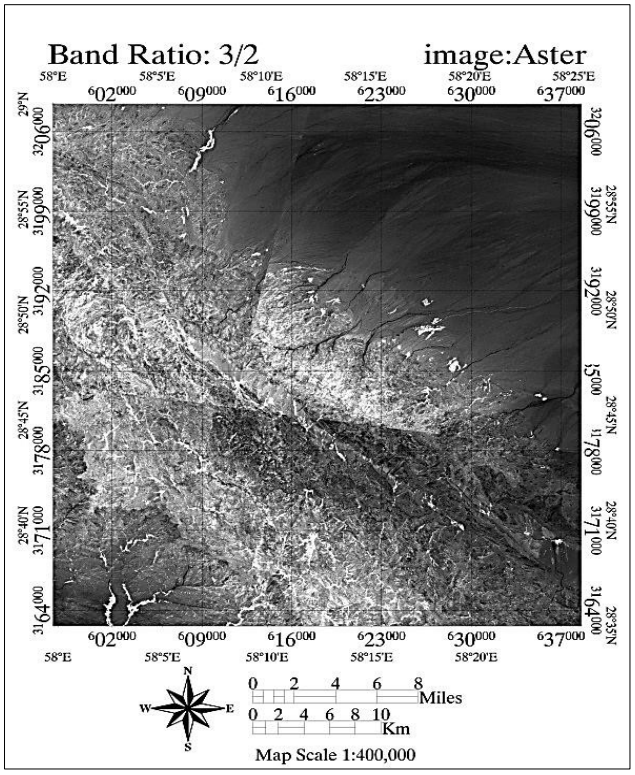

Fig 5. 3/2 band ratio to detect the vegetation in bright pixel in 1:100000 sheet of Jebal-Barez.

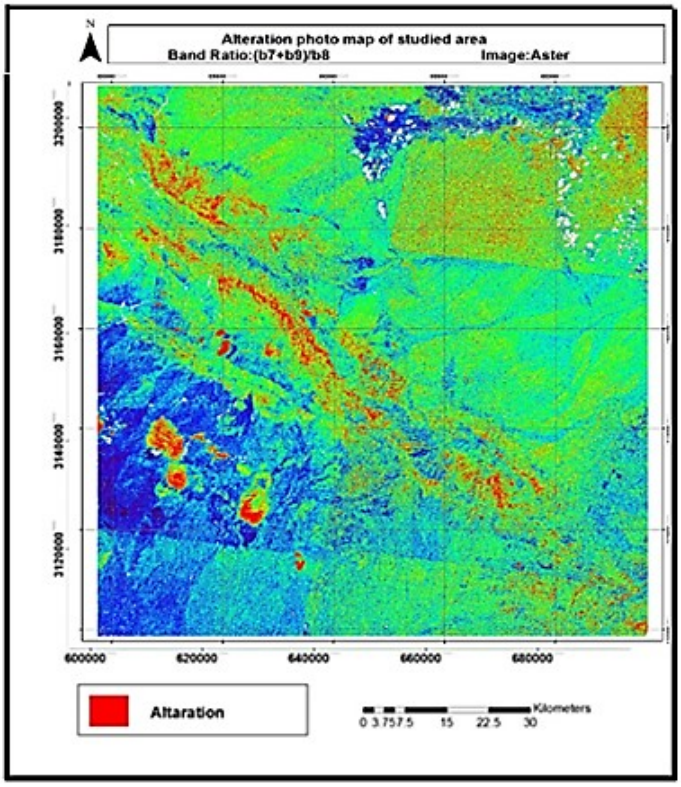

Fig 6. The propylitic alteration images prepared based on band ratio method.

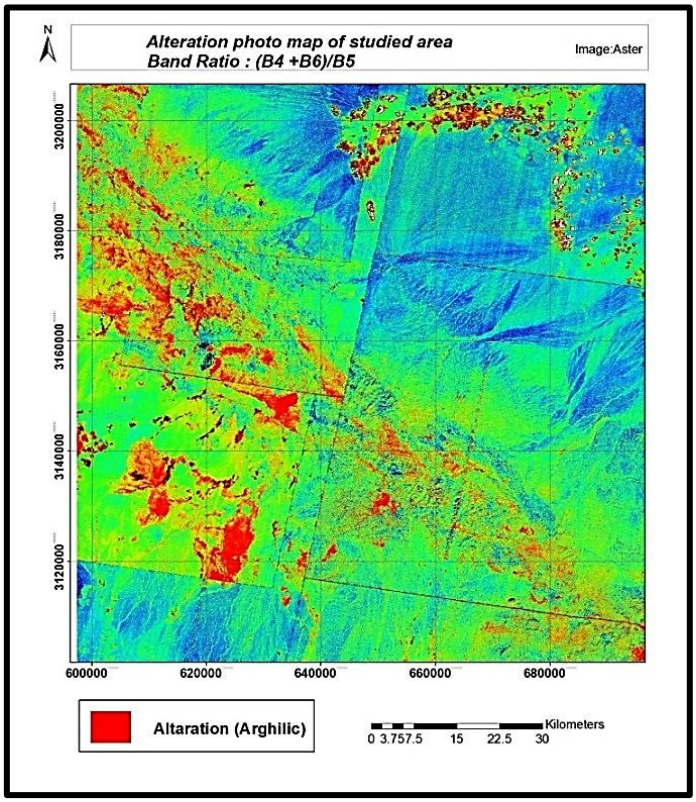

Fig 7. The argillic alteration images prepared based on band ratio method.

Table 4. The ASTER false colour composite 468

Details	Colour Composite		
	Red	Green	Blue
Phyllic and Argillic alterations: amethystine Propylitic alteration: Green Carbonate rocks: Yellow Carbonate metamorphic rocks and Dolomite rocks: Yellow and green (beside each other).	4	6	8

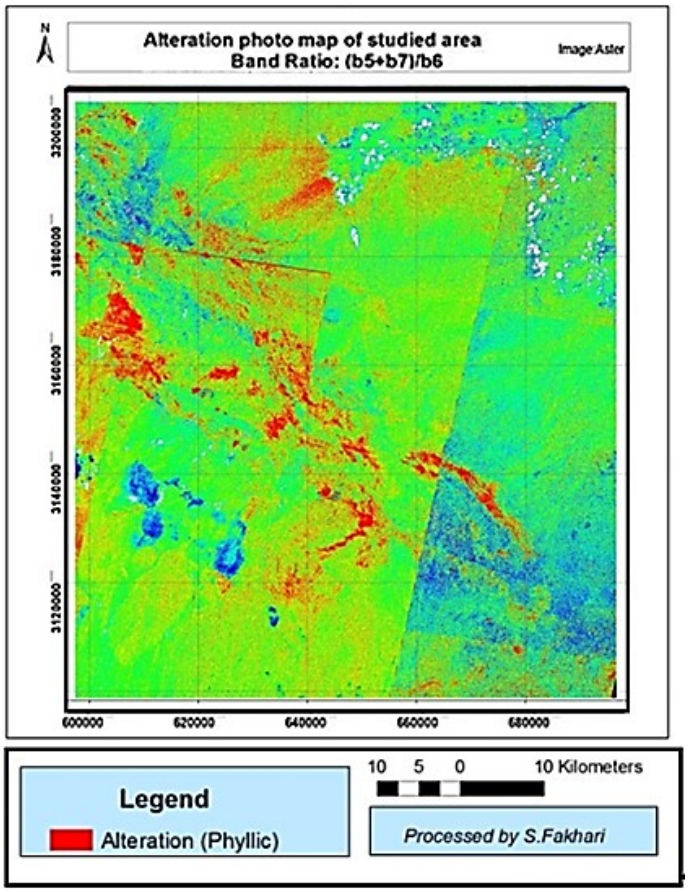

Fig 8. The phyllic alteration images prepared based on band ratio method.

2.4.2. False color composite

Remote sensing images have multi-bands, so one band processing cannot be effective for gathering information. For this reason, color composite was applied to identify minerals and other features. The creation of false color composite is based on known spectral properties of rocks and alteration mineral in relation to the selected spectral bands. In this study, three color composites were generated for the purpose of alteration and lithological mapping (Table 4). The ASTER (RGB: 468) false color composite 468 (RGB) images typically show argillic and phyllic altered rocks as amethystine tones, and propylitic altered rocks as green tones because of Al-O-H (at ASTER band six) and Fe-, Mg-O-H (at ASTER band eight) absorption features, respectively (Fig 9).

2.4.3. SAM

The SAM method is applied by many researchers in remote sensing studies for mineral exploration (Kruse et al. 1993; Tangestani et al. 2008; Azizi et al. 2010; Sojdehee et al. 2016). It is a physically-based spectral classification that uses an n-dimensional angle to match pixels to reference spectra. The algorithm determines the spectral similarity between the image and reference spectra by calculating and comparing the cosine value of these two spectra. High cosine values between the two spectra indicate high similarity, whereas low values indicate low similarity (Kruse et al., 1993; Honarmand et al. 2011; Beiranvandpour and Hashim 2011; Ting Qiu et al. 2015). The cosine value can be computed using Equation. 1, where n_b, t_i and r_i are number of bands, reflectance of band *i* for image spectrum, and

reflectance of band i for reference spectrum, respectively as follows:

$$cos\alpha = \frac{\sum_{i=1}^{nb} t_i r_i}{\sqrt{\sum_{i=1}^{nb} t_i^2}\sqrt{\sum_{i=1}^{nb} r_i^2}} \quad (1)$$

In this study, the SAM method was implemented for 15 index minerals being indicators of different alteration faces using spectra from the imagery and the spectra of alteration minerals selected from the United States Geological Survey (USGS) spectral library and resampled to ASTER spectral resolution. The results via ASTER mineral mapping are depicted in Figs.9-13. Iron oxide-hydroxide including jarosite, goethite, hematite and limonite occur in most parts of the studied area while jarosite is more dominant in the central part (Fig 10). This mineral is present in advanced argillic alteration too and shows absorption depth at 2.2 µm due to the presence of hydroxyl ions (OH^-; Fig 10). Phyllic alteration with illite, pyrite, muscovite and quartz (Fig 10) and argillic alteration which consist of montmorillonite, kaolinite, halloysite and dickite are more widespread (Fig 10).

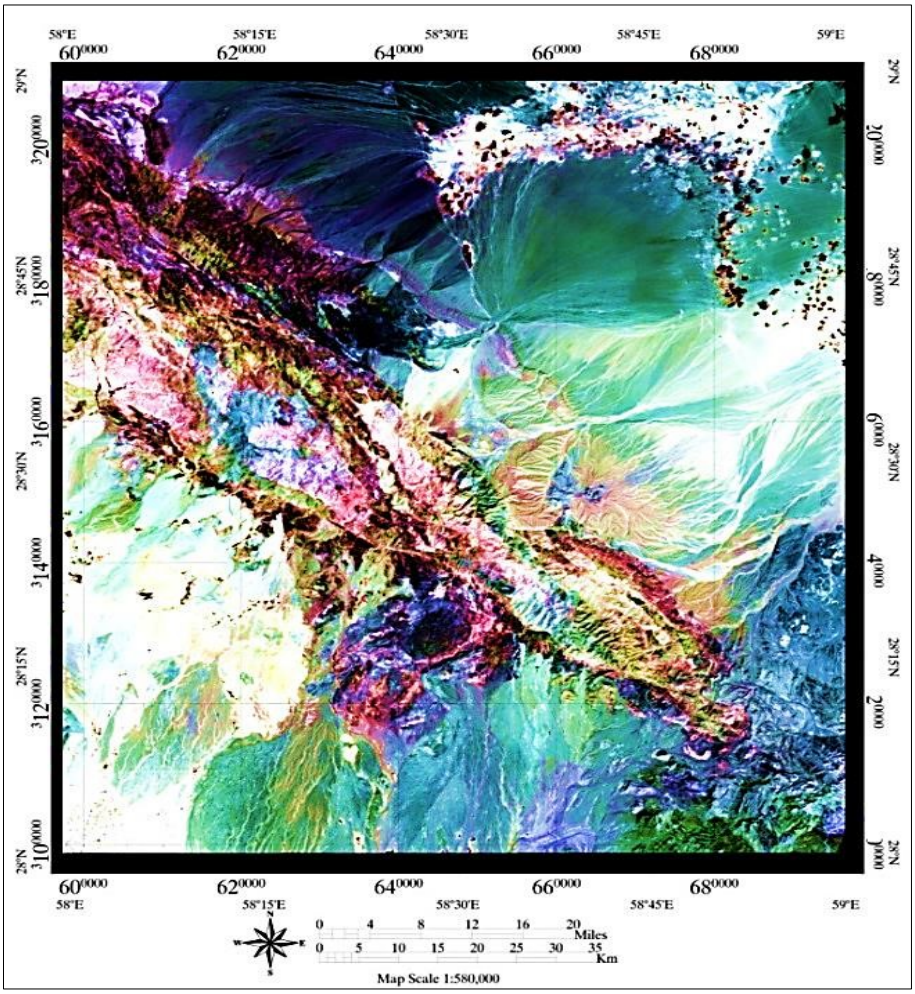

Fig 9. The results of False colour composite 468 (RGB) images on Jebal-Barez. Phyllic and argillic alterations in amethystine, propylitic alteration in Green and carbonate rocks in Yellow.

The clay minerals montmorillonite which showed absorption depth at 1.9 µm is more widespread (Yazdi et al. 2016; Fig 4). Propylitic alteration zones are less widespread than argillic alteration (Fig 10) and abundant along the fault zones. The overall distribution of these alterations based on SAM method shows the widespread alteration in SE part besides a completely altered zone in NW part which mostly consists of jarosite. Therefore, these domains require closer inspection, field study and sampling, as shown in Fig. 10.

3. Result and Discussion

In this study, three methods of ASTER processing are used and the results are presented in Figures 5 to 10. Based on band ratio method, 4/9 and 7/9 bands ratio have shown alteration, but in some cases, vegetation is the major problems for processing images.

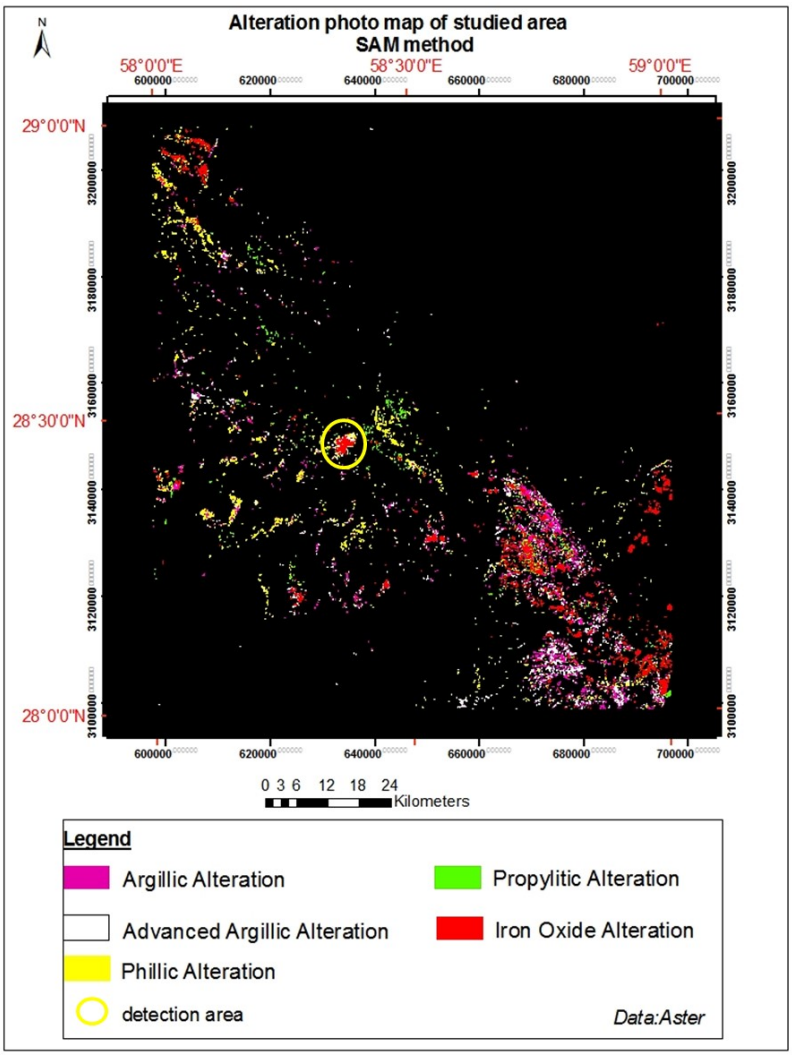

Fig 10. The image prepared based on SAM method for showing the final alteration map of the study area. Detection area contains all alteration zones with a circular structure.

However, 3/2 band ratio is utilized for identifying vegetation and musk it. In total, based on ASTER band ratio processing, alterations are spread in the area. Therefore, this area is one of the most potential areas for copper in SE Iran (Figs 6, 7 and 8). On the other hand, false color composite are used. In image processing ASTER (RGB: 468) false color composite shown phyllic and argillic alterations in amethystine. Moreover, propylitic alteration, carbonate and dolomite are situated on some places and they are also in green and yellow, respectively (Fig 9).

In SAM method, Iron oxide-hydroxide including jarosite, goethite, hematite and limonite are detected in most parts of the studied area while jarosite is more dominant in most parts (Fig 10). This mineral is present in advanced argillic alteration too (Fig 10) and shows absorption depth at 2.2 µm due to the presence of hydroxyl ions (OH^-; Fig 4). The phyllic alteration with illite, pyrite, muscovite and quartz (Fig 10) and argillic alteration consist of montmorionite, kaolinite, halloysite and dickite which are more widespread (Fig 10). The montmorionite which showed absorption depth at 1.9µm is more widespread (Yazdi et al. 2018). Moreover, propylitic alteration zones are less widespread than argillic alteration (Fig 10) and abundant along the fault zones. The overall distribution of these alterations based on SAM method indicates the presence of extensive phyllic and argillic alteration zones. The argillic alteration is surrounded by border zones of propylitic alteration (Fig 10). In addition, field observations have a correlation with results obtained from SAM method in the area since iron oxides, argillic alteration, and epidote as the main index of propylitic are obviously present in the NW and SE as depicted in Fig. 11. Therfore, to evaluate the alteration zones, field-checks have been verified.

For more detaile, all these methods detect the granodiorite intrusive rocks in NW of the studied area (Fig 12) which is completely altered and we called it "Detection area" as a target area (Fig 10). The combination of alteration zones in this area in order of frequency is jarosite sericite, quartz and

montemoriyonite which seem to indicate the iron oxide, phyllic, advanced argillic and argillic alteration respectively (Fig 12). Moreover, there is a loop system for alteration zones in this region which is a sign for porphyry system. Furthermore, advanced argillic areas in the plutonic rocks indicate potential for gold mineralization. Consequently, based on data processing which is used in this study, the "Detection area" as a massive granodiorite intrusion seems to be a potential area for Cu mineralization, so it needs more detailed exploration and excavation.

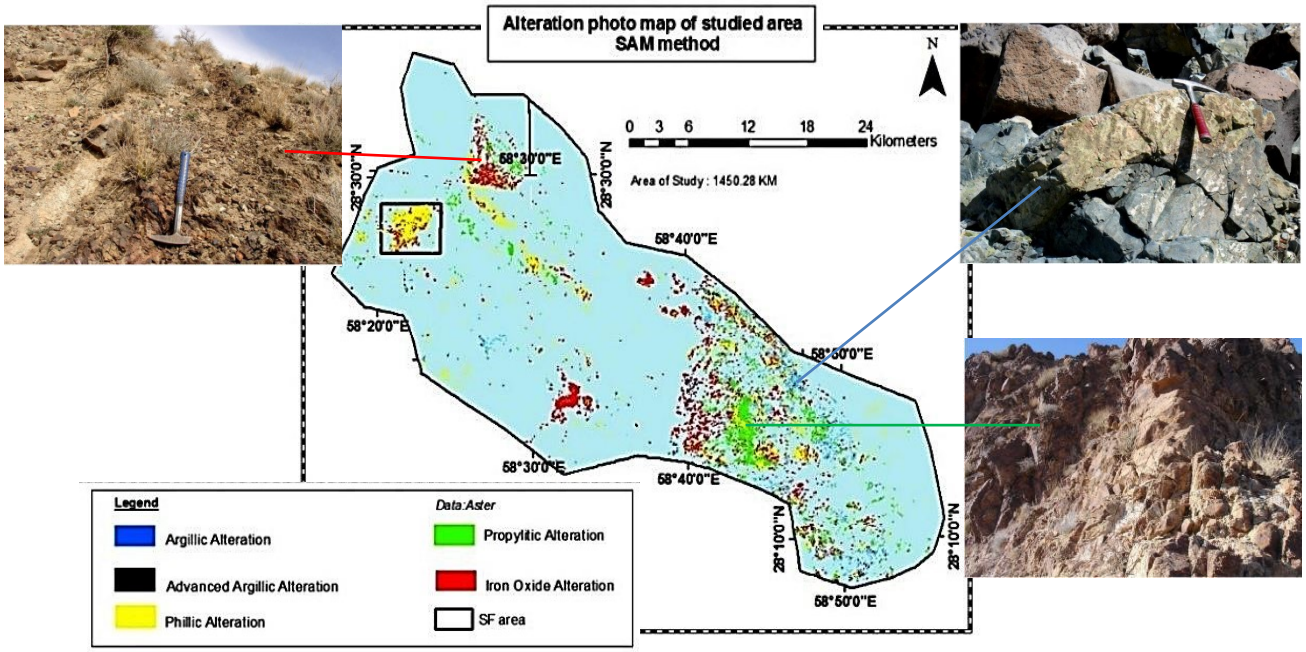

Fig 11. The final alteration map of the research area based on SAM method whit a) Iron Oxide, b) Argillic and c) Propylitic alteration field observations.

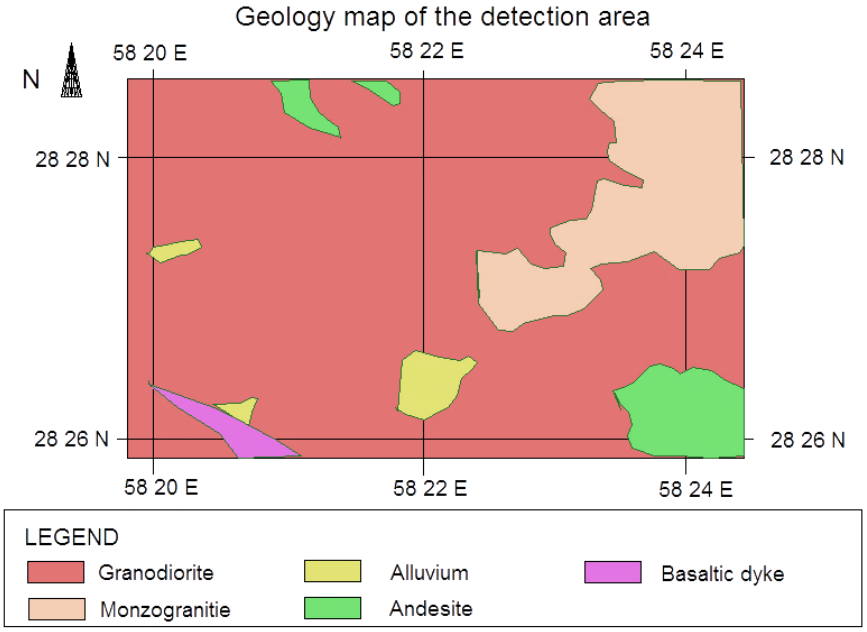

Fig 12. The geology map of the "Detection area". This area is a massive granodiorite intrusion, which is the main host rocks of Copper Porphyry mineralization.

4. Conclusions

ASTER images processing including band ratio, false color composite and SAM for mapping the region of hydrothermal alteration in Jebal-Barez region are accurate and helpful in detecting zones of phyllic, argillic and propylitic alterations, and also Fe-oxides, clays and copper minerals. The results of this study indicate the presence of extensive phyllic and argillic alteration zones. The argillic alterations are surrounded by border zones of propylitic alteration. This research shows that ASTER images processing can be useful and powerful tool in prospecting steps for those deposit types which have relation with alteration such as "Detection area" which is enhanced in this research as a more potential zone to explore Cu mineralization and is recommended for field survey.

Acknowledgments

The authors gratefully acknowledge the Hadid Gostar Sirjan Company for preparing all the data sets.

References

Afzal P, Eskandarnejad Tehrani M, Ghaderi M, Hosseini MR (2016) Delineation of supergene enrichment, hypogene and oxidation zones utilizing staged factor analysis and fractal modeling in Takht-e-Gonbad porphyry deposit, SE Iran. *Journal of Geochemical Exploration* 161: 119-127.

Alimohammadi M, Alirezaei S, Kontak DJ (2015) Application of ASTER data for exploration of porphyry copper deposits, A case study of Daraloo–Sarmeshk area, southern part of the Kerman copper belt, Iran, *Ore Geology Reviews* 70: 290 – 304.

Aramesh Asl, R., Afzal, P., Adib, A., Yasrebi, A.B., 2015. Application of multifractal modelling for the identification of alteration zones and major faults based on ETM+ multispectral data. *Arabian Journal of Geosciences* 8: 2997–3006.

Asadi S, Moore F, Zarasvandi A (2014) Discriminating productive and barren porphyrycopper deposits in the southeASTERn part of the central Iranian volcano–plutonic belt, Kerman region, Iran - A review, *Earth Sciences* 138:25–46.

Azizi H, Tarverdi M, Akbarpour A (2010) Extraction of hydrothermal alterations from ASTER SWIR data from east Zanjan, northern Iran, *Advances in Space Research* 46:99–109.

Beiranvandpour A, Hashim M, Marghany M (2011) Using spectral mapping techniques on short wave infrared bands of ASTER remote sensing data for alteration mineralmapping in SE Iran, *International Journal of Physical Sciences* 6:917–929.

Dimitrijevic MD (1973) Geology of Kerman region, Geological Survey of Iran, Report YU/52.

Daneshvar Saein, L., Afzal, P., 2017. Correlation between Mo mineralization and faults using geostatistical and fractal modeling in porphyry deposits of Kerman Magmatic Belt, SE Iran. Journal of Geochemical Exploration 181: 33-343.

Hedenquist JW, Arribas RA, Gonzalez-Urien E (2000) Exploration for epithermal gold deposits. In: Hagemann, S.G. (Ed.), Gold in 2000. *Reviews in Economic Geology* 13, 245-277.

Hezarkhani A (2006) Hydrothermal evolution of the Sar-Cheshmeh porphyry Cu–Mo deposit, Iran, evidence from fluid inclusions, *Journal of Asian Earth Sciences* 28: 409-422.

Holliday JR, Cooke DR (2007)Advances in geological models and exploration methods for copper±gold porphyry deposits, fifth decennial international conference on mineral exploration, Prospectors and Developers Association of Canada, Toronto, 791–809.

Honarmand M, Ranjbar H, Shahabpour J (2011) Application of Spectral Analysis in Mapping Hydrothermal Alteration of the Northwestern Part of the Kerman Cenozoic Magmatic Arc, Iran, *Journal of Sciences, Islamic Republic of Iran* 22: 221–238.

Kruse FA, Lefkoff AB, Boardman JB, Heidebrecht KB, Shapiro AT, Barloon PJ, Goetz A.F.H (1993)The Spectral Image Processing System (SIPS) - interactive visualization and analysis of imagingspectrometer data, *Remote Sensing of Environment* 44: 145–163.

Lang JR, Stanley CR, Thompson JFH (1995) Porphyry copper-gold deposits related to alkalic igneous rocks in the Triassic-Jurassic arc terranes of British Columbia: *Arizona Geological Society Digest* 20:219–236.

Lowell JD, Guilbert JM (1970) Lateral and vertical alteration-mineralization zoning in porphyry ore deposits, *Economic Geology* 65: 373–408.

Pazand K, Javanshir AR (2015) Orientation hydrogeochemical survey in Jebal-e-Barez area, SE Iran. *Sustainable Water Resources Management* 1: 167-180.

Mars JC, Rowan LC (2006) Regional mapping of phyllic- and argillicaltered rocks in the Zagros magmatic arc, Iran, using Advanced Spaceborne Thermal Emission and Reflection Radiometer (ASTER) data and logical operator algorithms 2:161–186.

Mars JC, Rowan LC (2010) Spectral assessment of new ASTER SWIR surface reflectance data products for spectroscopic mapping of rocks and minerals, *Remote Sensing of Environment* 114: 2011–2025.

Meyer C, Hemley JJ (1967) Wall rock alteration. In: Barnes HL (ed.) Geochemistry of hydrothermal ore deposits. Holt Rinehart and Winston, New York, 166–235.

Rowan L, Hook SJ, Abrams MJ, Mars JC (2003) Mapping hydrothermally altered rocks at Cuprite, Nevada, using the Advanced Spaceborne thermal emission and reflection radiometer (ASTER), a new satellite-imaging system. *Economic Geology* 98: 1019–1027.

Rowan LC, Schmidt RG, Mars JC (2006) Distribution of hydrothermally altered rocks in the Reko Diq, Pakistan mineralized area based on spectral analysis of ASTER data. *Remote Sensing of Environment* 104: 74–87.

Sabins FF (1999) Remote sensing for mineral exploration, *Ore Geology Reviews* 14: 157– 183.

Shafiei B (2010) Lead isotope signatures of the igneous rocks and porphyry copper deposits from the Kerman Cenozoic magmatic arc (SE Iran), and their agmatic–metallogenetic implications, *Ore Geology Reviews* 38: 27–36.

Shafiei B, Haschke M, Shahabpour J (2009) Recycling of orogenic arc crust triggers porphyry Cu mineralization in Kerman Cenozoic arc rocks, southeASTERn Iran, *Mineralium Deposita* 44:265–283.

Sillitoe RH (2002) some metallogenic features of gold and copper deposits related to alkaline rocks and consequences for exploration. *Mineralium Deposita* 37:4–13.

Sillitoe RH (2010) Porphyry copper systems. *Economic geology* 105:3–41.

Sillitoe RH, Gappe IM (1984) Philippine porphyry copper deposits: Geologic setting and characteristics: Bangkok, Thailand. United Nations ESCAP, CCOP *Technical Publication* 14:68- 89.

Sojdehee M, Rasa I, Nezafati N, Vosoughi Abedini M (2016) Application of spectral analysis to discriminate hydrothermal alteration zones at Daralu copper deposit, SE Iran, *Arabian Journal of Geosciences* 9: 41–53.

Tangestani MH, Mazhari N, Agar B, Moore F (2008) Evaluating Advanced Spaceborne Thermal Emission and Reflection Radiometer (ASTER) data for alteration zone enhancement in a semi-arid area, northern Shahr–e–Babak, SE Iran, *International Journal of Remote Sensing* 29: 2833–2850.

Ting Qiu J, Zhang C, Hu X (2015) Integration of concentration-area fractal modelling and spectral angle mapper for ferric iron alteration mapping and uranium exploration in the Xiemisitan Area, NW China, *Remote Sensing* 7:13878–13894.

Yazdi Z, Jafari-Rad A, Aghazadeh M, Afzal P (2018) Alteration Mapping for Porphyry Copper Exploration Using ASTER and QuickBird Multispectral Images, Sonajeel Prospect, NW Iran. *Journal of the Indian Society of Remote Sensing* 46 (10): 1581–1593.

Zoheir B, Emam A (2012) Integrating geologic and satellite imagery data for highresolution mapping and gold exploration targets in the South EASTERn Desert, Egypt. *Journal of African Earth Sciences* 66–67.